NSF Research Experience for Undergraduates

University of Florida

Caela Barry

Investigating Control Strategies for the Advanced VIRGO EIB IP using SimMechanics

Supervisor: David S. Rabeling

1 Introduction

1.1 Gravitational Waves and Interferometric Detection

Gravitational waves are quadrupolar ripples in spacetime originating from sources containing non-spherical dynamics, such as compact binaries, rotating neutron stars, and massive stellar core collapse events. A stochastic background of residual gravitational waves, analogous to the cosmic microwave background, is expected to provide insight into the earliest history of the universe. The existence of gravitational waves has been predicted by Einstein's Theory of General Relativity, but direct detection has not yet been achieved.

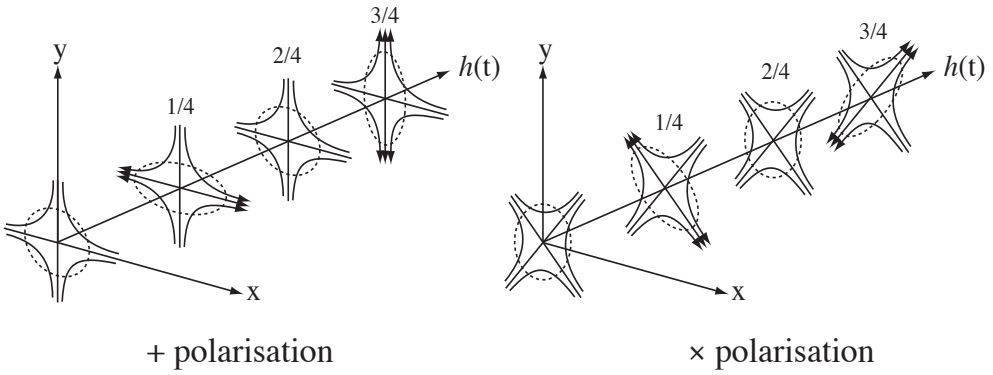

Figure 1: Gravitational wave component polarizations and their effect on a circular ring of particles in the wave path. Any gravitational wave signature will be describable as a linear combination of these two polarizations with respect to the detector.

The primary reason for the elusiveness of gravitational waves is their weak interaction with matter. The ability to accurately measure — and rule out non-GW sources of — displacements on the order of 10^{-19} meters is an exceptionally challenging prerequisite for detection. Although no observatory has registered a GW event thus far, experimental research has pushed design sensitivity of the upcoming generation of interferometers to a level at which detection events are predicted to occur tens of times per year.

Gravitational waves are conventionally divided into ultra-low, very low, low and high frequency bands. The VIRGO experiment and its successors have been designed to observe the high spectrum, from roughly 10Hz to 2000Hz. It is important to note that the waveform h measured in a gravitational wave detector falls off as $\frac{1}{r}$, where r is distance from the wave source, meaning that a sensitivity improvement of one order of magnitude increases the volume of observable space by a factor of 1000. LIGO and VIRGO upgrades implemented in the next five years will provide just such an expansion.

A typical interferometric gravitational wave detector, such as VIRGO, has two perpendicular arms, each of which houses a meticulously tuned Fabry-Perot cavity. These are several meters to kilometers long (the VIRGO and large LIGO interferometers, for instance, have arms of length 3 km and 4 km respectively, although the effective length of the test beams is on the order of 100 times larger thanks to internal reflection in the Fabry-Perot cavities). A laser beam is injected at left in figure 2, divided by a beam splitter, and directed into the interferometer arms. The

phase of the light is such that it interferes destructively in the space between the beam splitter and the photodiode (PD) at the bottom of the diagram. Differential changes in arm length alter this interference and allow a light signal to reach the photodiode.

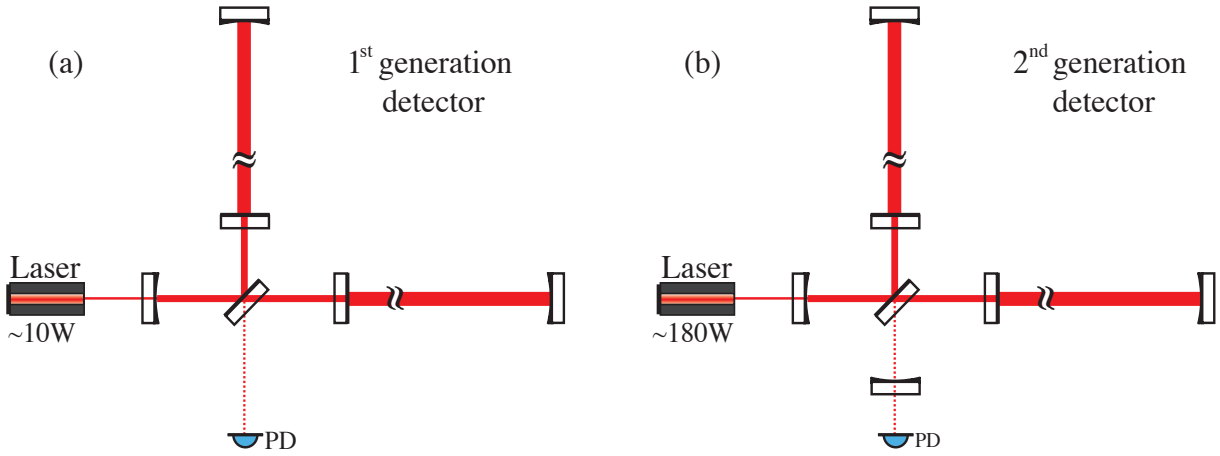

Figure 2: Simplified layouts of VIRGO and VIRGO+, respectively. Advanced VIRGO will be schematically similar to its 2nd generation predecessor, with an order of magnitude increase in sensitivity arising from new attenuation systems, including EIB-SAS, and improved mirror coating treatments.

1.2 The EIB-SAS Table for Advanced VIRGO

Seismic and human noise cause much larger displacement signals than are expected to be induced by gravitational waves. In Advanced VIRGO, the External Injection Bench Seismic Attenuation System (EIB-SAS) discussed here will be one of many attenuation systems developed to isolate components from unwanted disturbances. The EIB-SAS, shown in figure 3, is a six-degree-of-freedom seismic isolation table developed at Nikhef to isolate the EIB of Advanced VIRGO from seismic and other noise. From base to top it consists of an inverted pendulum layer, a 'spring box' layer of GAS filters, and the optical bench surface.

Despite the fact that the SAS table is an effective attenuator of seismic noise, it has a number of internal modes which can be problematic. Although the SimMechanics simulation tool, described in section 3, does not support modeling of structural resonances, the EIB-SAS internal modes have been simulated by Eric Hennes of Nikhef using the finite element package MSC Marc. This report investigates strategies for damping these modes and the inherent resonances of the triple inverted pendulum through the implementation of either passive shunt damping units or active feedback control loops in key locations throughout the apparatus.

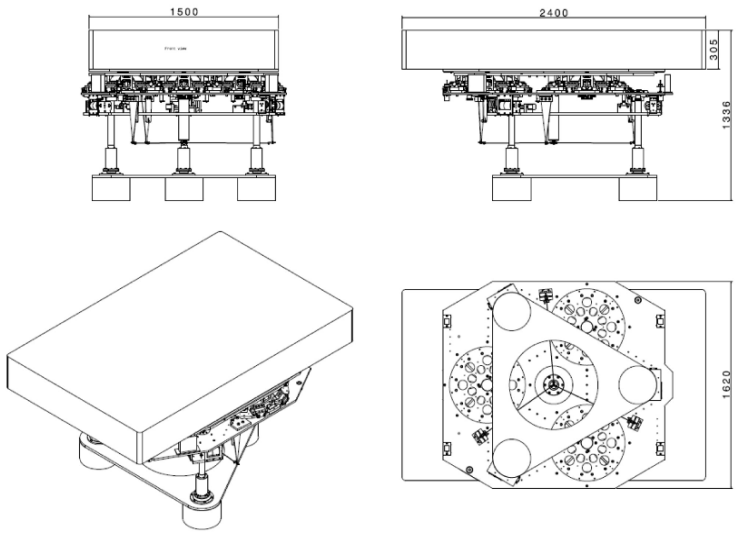

Figure 3: Front, side, perspective, and top views of the EIB-SAS

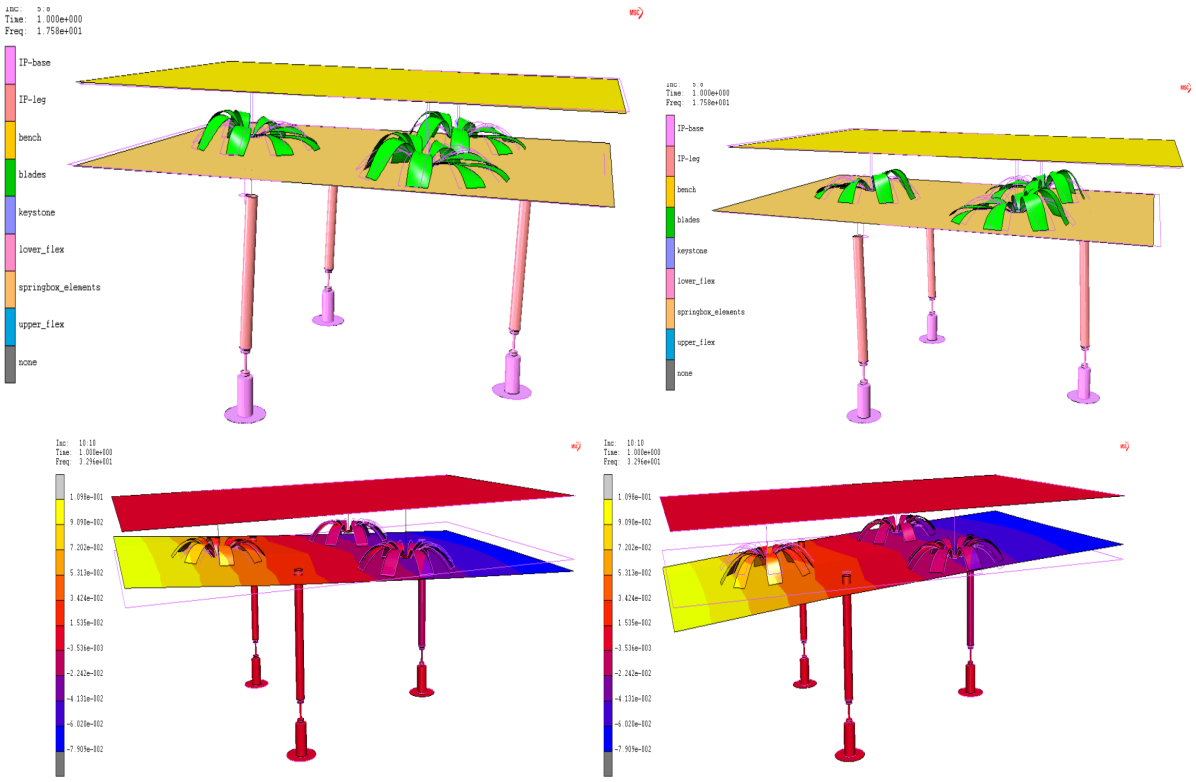

Figure 4: Examples of EIB-SAS structural resonances

2 Suspension Attenuators and Control Systems

A simple harmonic oscillator, such as a spring-mass system or inverted pendulum, is a natural attenuator of seismic noise whose frequency is higher than the resonant frequency ω_0 of the system. Noise with $\omega < \omega_0$ propagates along the spring or pendulum with no phase lag or change in amplitude; in this frequency range the oscillator behaves like a rigid body.

Excitation at the resonant frequency leads to a phase lag of 90 degrees, which causes energy added via a force at the suspension point to contribute continuously to the oscillatory motion of the system. As a result, the test mass oscillates around its rest position with increasing amplitude. In an attenuation device, resonant behavior must be controlled by some method of auxiliary damping.

For $\omega > \omega_0$, the phase lag between input and output is 180 degrees. In this situation we can write the kinetic energy of the system as the test mass passes through its rest position as

$$E_k = \frac{1}{2}mv^2 = \frac{1}{2}mA^2\omega^2 \tag{1}$$

Equation 1 shows that for a given energy E_k, A decreases as $\frac{1}{\omega^2}$, where A is the amplitude of the test mass oscillation. In other words, the simple harmonic oscillator is a passive, mechanical low-pass noise filter.

2.1 The Classical Spring-Mass System

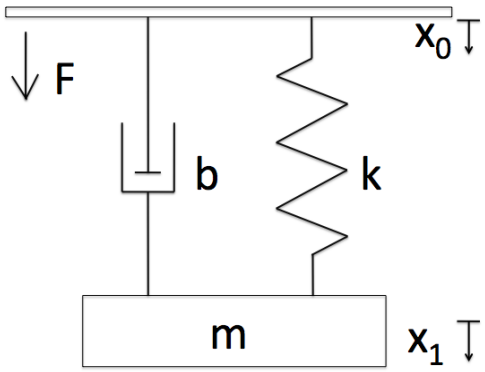

Figure 5: A classic example of simple harmonic oscillation: the damped spring-mass system.

The natural dynamics of a system composed of a mass suspended vertically from a spring with one end fixed at a point are described by the following expressions:

In the time domain,

$$\frac{F}{m} + \ddot{x}_1 = \frac{-k}{m}(x_1 - x_0) - \frac{b}{m}(\dot{x}_1 - \dot{x}_0) \tag{2}$$

where k is the spring constant and b the viscous damping constant of the system. After a Fourier transform, the same relation in the frequency domain is

$$\frac{\mathcal{F}}{m} - \left(\omega_0^2 + \frac{ibw}{m}\right)\mathcal{X}_0 = \left(\omega^2 - \frac{ibw}{m} - \omega_0^2\right)\mathcal{X}_1 \tag{3}$$

Active damping may be introduced in order to suppress the noise amplification introduced at ω_0, a possibility we will examine in some detail as an example of feedback control in section 3.1.

2.2 Inverted Pendulum Theory

Here we derive the dynamics of an ideal inverted pendulum system. Figure 6 shows the inverted pendulum where we designate the angles of rotation as follows: θ for the suspension point, γ for the center of mass of the pendulum leg, and β for the end of the pendulum to which the mass is fixed. L_1 refers to the length of the pendulum leg; L_2 is the length from the suspension point to the leg center of mass ($L_2 = L_1/2$ for a leg of uniformly distributed mass). Similarly, x_0, x_1, and x_2 denote the x-coordinates of the suspension point, test mass, and leg COM, respectively, and J_0, J_1 and J_2 are their moments of inertia. m_1 signifies the test mass and m_2 the mass of the pendulum leg.

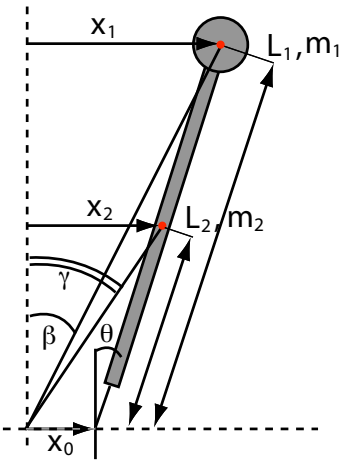

Figure 6: Inverted pendulum lengths, masses and angles

Using the definitions above and applying small angle approximations, the IP dynamics can be described by:

$$\tau = \tau_{inertial} + \tau_{spring} = 0 \tag{4}$$

$$\tau_{inertial} = J_0\ddot{\theta} + J_1\ddot{\gamma} + J_2\ddot{\beta} \tag{5}$$

$$\tau_{spring} = m_1 g(x_1 - x_0) + m_2 g(x_2 - x_0) - k\theta \tag{6}$$

$$J_1 = m_1 L_1^2 \tag{7}$$

$$J_2 = m_2 L_2^2 \tag{8}$$

$$\theta = \frac{x_1 - x_0}{L_1} \tag{9}$$

$$\gamma = \frac{x_1}{L_1} \tag{10}$$

$$\beta = \frac{x_2}{L_2} = \frac{2x_2}{L_1} \tag{11}$$

The horizontal displacements of the suspension point, leg COM, and test mass are related by the expression

$$x_2 - x_0 = \frac{L_2}{L_1}(x_1 - x_0) \tag{12}$$

and the equations of horizontal motion for the stable system are

$$\tau_{inertial} = \left(m_1 + \frac{m_2}{4} + \frac{J_0}{L_1^2}\right)\ddot{x}_1 + \left(\frac{m_2}{4} - \frac{J_0}{L_1^2}\right)\ddot{x}_0 \tag{13}$$

$$\tau_{spring} = k\frac{(x_1 - x_0)}{L_1} - g\left(m_1 + \frac{m_2}{2}\right)(x_1 - x_0) \tag{14}$$

We combine equations 4, 13, and 14 to obtain

$$\left(m_1 + \frac{m_2}{4} + \frac{J_0}{{L_1}^2}\right)\ddot{x}_1 + \left(\frac{m_2}{4} - \frac{J_0}{{L_1}^2}\right)\ddot{x}_0 = \frac{k}{{L_1}^2}(x_1 - x_0) - \frac{g}{L_1}\left(m_1 + \frac{m_2}{2}\right)(x_1 - x_0) \tag{15}$$

Rewriting this relation in the frequency domain ($\ddot{x} = i\omega^2 x$), we have the transfer function

$$\frac{x_1}{x_0} = \frac{{\omega_0}^2 - \omega^2\beta}{{\omega_0}^2 + \omega^2} \tag{16}$$

where

$$\omega_0^2 = \frac{\frac{k}{{L_1}^2} - \frac{g}{L_1}(m_1 + \frac{m_2}{2})}{m_1 + \frac{m_2}{4} + \frac{J_0}{{L_1}^2}} \tag{17}$$

$$\beta = \frac{\frac{m_2}{4} + \frac{J_0}{{L_1}^2}}{m_1 + \frac{m_2}{4} + \frac{J_0}{{L_1}^2}} \tag{18}$$

Each inverted pendulum in the EIB-SAS table is modified by the addition of a counterweight near its suspension point. Extending the analysis to include this information, the stable system is described by the equation

$$\tau = \tau_{p_{spring}} + \tau_{p_{inertial}} + \tau_{cw_{spring}} + \tau_{cw_{inertial}} = 0 \tag{19}$$

where subscript p denotes τ for the upper pendulum and load mass (as derived above) and subscript cw identifies torque components introduced by the counterweight apparatus. The contribution of translational motion is accounted for by measuring θ, β and γ from a reference point which does not move with the pendulum.

The addition of a counterweight provides a means for adjusting the leg center of percussion. The center of percussion, or point on the pendulum leg around which the system rotates when an external force is applied, determines the lateral motion of the top mass resulting from a displacement x_0 of the suspension point, approximated by

$$x_1 = -\beta x_0 \tag{20}$$

As β goes to zero, so does x_1; therefore in an ideal attenuation system we have $\beta = 0$. We can attain low β values by minimizing the mass m_2 of the pendulum leg and using a counterweight to tune the inertia of the system. The effect of β on the transfer function of an inverted pendulum system can be seen in figure 7.

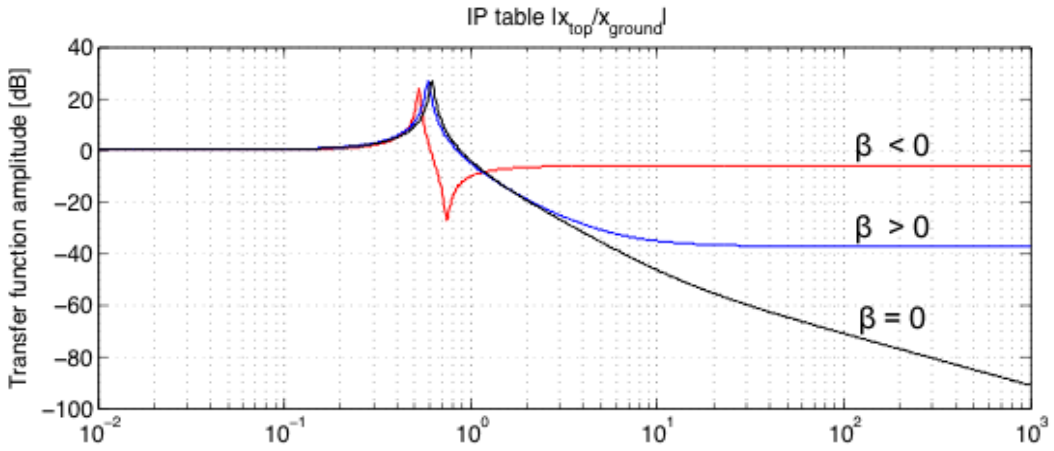

Figure 7: Influence of the center of percussion term β on an inverted pendulum transfer function. The horizontal axis measures frequency (Hz). The transfer function of an ideal pendulum, where $\beta = 0$, is plotted in black. When $\beta < 0$, plotted in red, the center of percussion introduces a dip into the transfer function, followed by a leveling-off. The blue plot shows the flattening of the transfer function for $\beta > 0$.

2.3 Force Feedback Control

A gravitational wave detector relies on a myriad of feedback control systems to suppress the interference of otherwise dominant noise. In general, the role of each of these control systems is to prevent a physical parameter from deviating from a predefined value, or 'set point', in the presence of forces that may influence that parameter in a problematic way. We have already introduced an example of a system transfer function, a mathematical expression that fully characterizes the system we want to control, in our derivation of inverted pendulum dynamics. Equation 16 gives the complex response function of the system in the frequency domain as the ratio of the system's output over its input. As discussed in section 2, noise is enhanced rather than suppressed at any eigenfrequecy ω_0 of the system. Our goal is to reduce this amplification without adversely affecting the noise filtering capabilities of the overall system. Previous investigation of the EIB-SAS table by finite element methods has identified many internal modes at frequencies ranging from 0.1 Hz to 100 Hz. In the feedback control loops considered here, sensors will measure deviation from a desired value (in this case, position, velocity, or acceleration) at a resonating point in the system and produce a signal that uses an opposing force to restore the table to its desired position.

In order for damping of mechanical system resonances to be possible, the control loop must exhibit stable behavior itself. The stability of the control loop depends on the phase of the open-loop transfer function of the system, so called as a result of the conceptual point that in calculating this function we 'break' the loop at an arbitrary point and multiply the transfer functions of its components together. The phase lag, or phase at any unity gain point, of the system must not be less than -180 degrees with respect to the reference phase. Phase lag outside of this range means that feedback force is applied at the wrong time in the oscillation cycle of the test mass,

contributing to noise amplification instead of canceling it out, and the system becomes unstable. The open-loop gain of our system is obtained by taking the product of the transfer functions of the plant (EIB-SAS table), the sensor, and a control filter that adjusts the feedback variable to exactly counteract the disturbance. We label these functions G, s^2, and C respectively.

The closed-loop transfer function models the full feedback behavior of the system, including the influence of the free-running (uncontrolled) output processed by the corrective components. For a (semi-)passive noise attenuation system such as the EIB-SAS, the reference signal to be tracked is zero — feedback holds isolated elements in a near-motionless state — and the closed-loop TF takes the form

$$\frac{x_1}{x_0} = \frac{G}{1 + Gs^2C} \tag{21}$$

where Gs^2C is the open-loop transfer function of the system, and the feedback filter C is given by

$$C = \frac{s + \omega_0}{(s + \omega_1)(s + \omega_2)} \tag{22}$$

where ω_1 and ω_2 are corner frequencies of the feedback transfer function gain. Knowing that the desired value of $\frac{x_1}{x_0}$ is zero, we can see from equation 21 that high open-loop gain is a key characteristic of an effective attenuation network.

It is worth noting that, in some cases, force feedback is not necessary for all frequency bands and an alternative, passive damping system should be considered. Passive damping has advantages as an analog process: the system is not dependent on computing or power-generating robustness to sustain its stability, and the lack of an engineered sensor-actuator-driver sequence means less noise is introduced into the system during the feedback cycle.

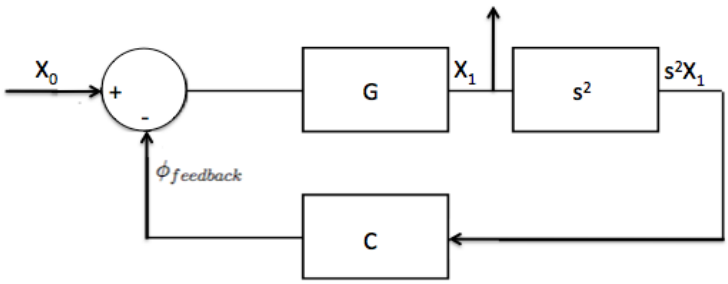

Figure 8: Visualization of the control loop discussed in equations 21 and 22. $\phi_{feedback}$ represents the feedback force.

3 Simulations using SimMechanics

SimMechanics, a specialized simulation environment in MatLab's SimScape physical modeling package, provides an extensive selection of "blocks" from which complex systems can be assembled. These represent machine components, such as joints, spring & damper elements, sensors, actuators, and inertial bodies, to which physical characteristics can be ascribed. In order to effectively

simulate the effects of the SAS table it is useful to construct modular damping units that are more complex and problem-specific than those included in the software package but still simple and customizable enough to be treated as building blocks themselves. In addition to the damped spring-mass system and solenoid actuator/shunt damper described in these examples, EIB-SAS modeling is simplified by the development of a block comprised of an inverted pendulum mounted on a flex joint and outfitted with a counterweight arrangement.

3.1 An Example of Active Attenuation: Sky-Hook Damping

We have already reviewed the natural motion of a mass-spring system suspended vertically from a fixed point, described by equation 3. In sky-hook damping, a feedback control loop is used to actively damp the resonance of such an arrangement. Using the SimMechanics software, the oscillating body is tracked by a motion sensor that produces a bundled signal containing position, velocity and acceleration information. Some or all of this information is treated as input for a compensator loop whose purpose is to maintain the stability of the system at resonant frequency. In the model shown here, acceleration along the vertical axis is extricated from the sensor signal, processed by a transfer function, and amplified by a variable gain G before re-entering the system as a corrective force via an actuator. The damping feedback function is chosen according to equation 22; effectiveness of damping varies as a function of G.

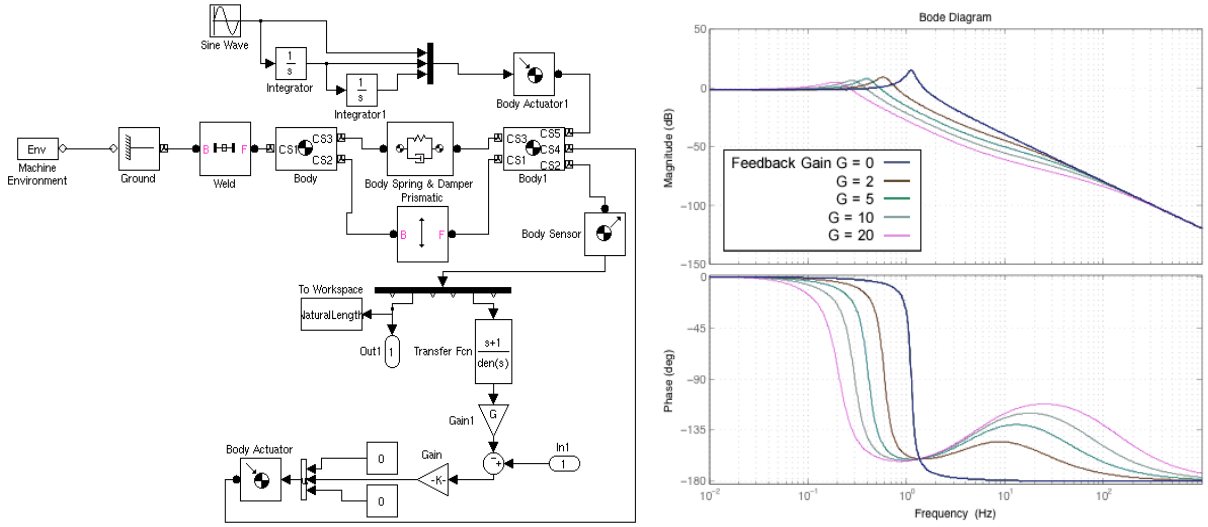

Figure 9: Modeling a sky-hook damping system in SimMechanics. **Left:** The oscillator-feedback system; **Right:** Bode plots of damping with G=0, 2, 5, 10, 20. G=0 (undamped system) is plotted in blue, G=20 in magenta.

3.2 An Example Of Passive Attenuation: Electromagnetic Shunt Damping

In electromagnetic shunt damping, energy transferred by the relative motion between system components is harnessed as induced electromotive force (EMF) rather than as the physical push of one surface against another. The EMF can be diffused in a coupled shunt circuit, quickly draining

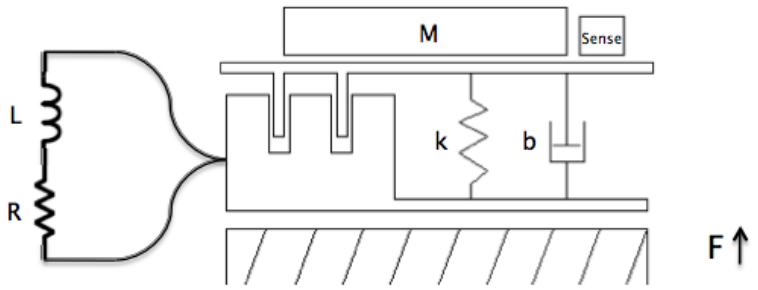

Figure 10: Schematic diagram of a solenoid connected in series to an RL shunt. Spring and damper elements k and b represent oscillatory properties of the resonating physical system; the electrical system dynamics can also be described by a stiffness k_{sys} and damping constant b_{sys}, discussed later in this section.

energy from the moving part and guiding the system back to equilibrium. This type of energy exchange is facilitated by a solenoid, composed of a coil of radius r, mounted on the axis of translational motion of part of the machine to be stabilized, and a ferromagnetic slug affixed to the facing surface of an adjacent part (or, in this case, an external frame of reference). The damping effects of this arrangement are modeled according to the following process:

When a disturbance is introduced into the system, the relative velocity $\dot{x}$ between the magnetic slug and the solenoid coil is processed by a motion sensor. Multiplication of the $\dot{x}$ signal by a transducer constant T_v models the induced EMF in the coil (measured in volts):

$$V = T_v(\dot{x}_{slug} - \dot{x}_{coil}) \tag{23}$$

where, for a coil of radius r, with N turns, and a slug with magnetic field B,

$$T_v = 2\pi r N B \tag{24}$$

A transfer function Y representing both the intrinsic admittance of the coil and the admittance of the shunt is applied to the voltage signal to produce the current generated by the relative motion of the magnet and coil:

$$I = -YV \tag{25}$$

where

$$Y = \frac{1}{Z} = \frac{1}{R + Ls} \tag{26}$$

$$R = R_{system} = R_{coil} + R_{shunt} \tag{27}$$

$$L = L_{system} = L_{coil} + L_{shunt} \tag{28}$$

The current I in the coil introduces a magnetic field which repels the slug in accordance with Lenz's laws, thereby resisting its advance into the coil and attenuating the disturbance. The stabilizing electromagnetic force is calculated as

$$F_{induced} = T_v I \tag{29}$$

The shunt circuit acts as a low-pass filter. Required damping and frequency range tuning are attained by choosing optimum values for R_{shunt} and L_{shunt}, respectively, when designing the shunt circuit. L_{shunt} is typically somewhat limited by physical design practicalities; For a solenoid with a given L_{shunt} and return spring constant k damped by an RL circuit, power dissipation can be optimized by calculating R_{shunt} according to the following formulas:

$$R_{opt} = L\left(\frac{\Omega_0^2}{\sqrt{\omega_0 \Omega_0}}\right) \tag{30}$$

$$\Omega_0^2 = \omega_0^2\left(1 + \frac{T_v^2}{kL}\right) \tag{31}$$

The shunt system can also be characterized in mechanical terms. The direct roles of R and L in controlling equivalent system stiffness k_{sys} and damping coefficient b_{sys} are given below:

$$k_{sys} = \frac{T_v^2}{L} = \omega_0^2 m \tag{32}$$

$$b_{sys} = \frac{T_v^2}{R} \tag{33}$$

It should be noted that the direct correlation between stiffness and resonant frequency in equation 32 can be seen in the vertical gap between the $R = 0.001\Omega$ and $R = 5\Omega$ plots in figure 11. Higher stiffness means that greater force is required to achieve the same displacement, hence the force to displacement transfer function has a lower overall amplitude in the stiffer $R = 0.001\Omega$ case.

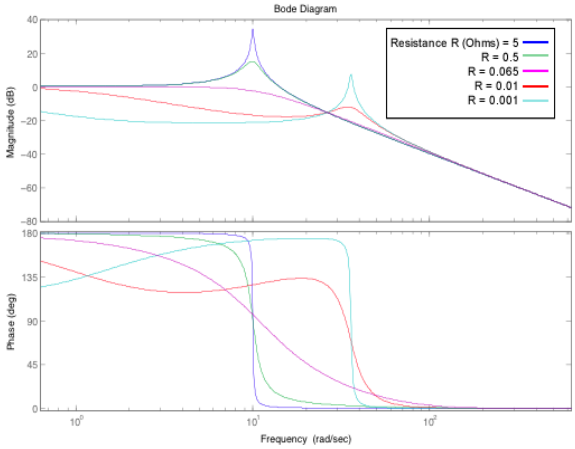

Figure 11: Bode plots of the force to displacement transfer function for SimMechanics model of a solenoid and shunt damping system. Graphs are shown for $R_{shunt} = 0.001$ (cyan), 0.01, 0.065, 0.5, and 5 (blue) Ω; L_{shunt} is held constant at 22mH. Optimized $R_{shunt} = 0.065\ \Omega$ shown in magenta.

3.3 Modeling the Inverted Pendulum

Since SimMechanics does not support modeling of the internal dynamics of bodies, the flex beam at the suspension point of the pendulum cannot be directly simulated using this software. Its

effect on the system can, however, be replicated using SimMechanics components. The flex beam is represented by a joint element characterized by two degrees of rotational freedom (pitch and roll). The material properties of the beam are converted to a rotational stiffness, which is then applied to both degrees of freedom via a joint spring & damper condition in the model. Body blocks provide coordinate systems for attaching the flex beam to the pendulum and counterweight legs and anchoring the entire apparatus to a ground component. The full inverted pendulum assembly is shown in figure 12.

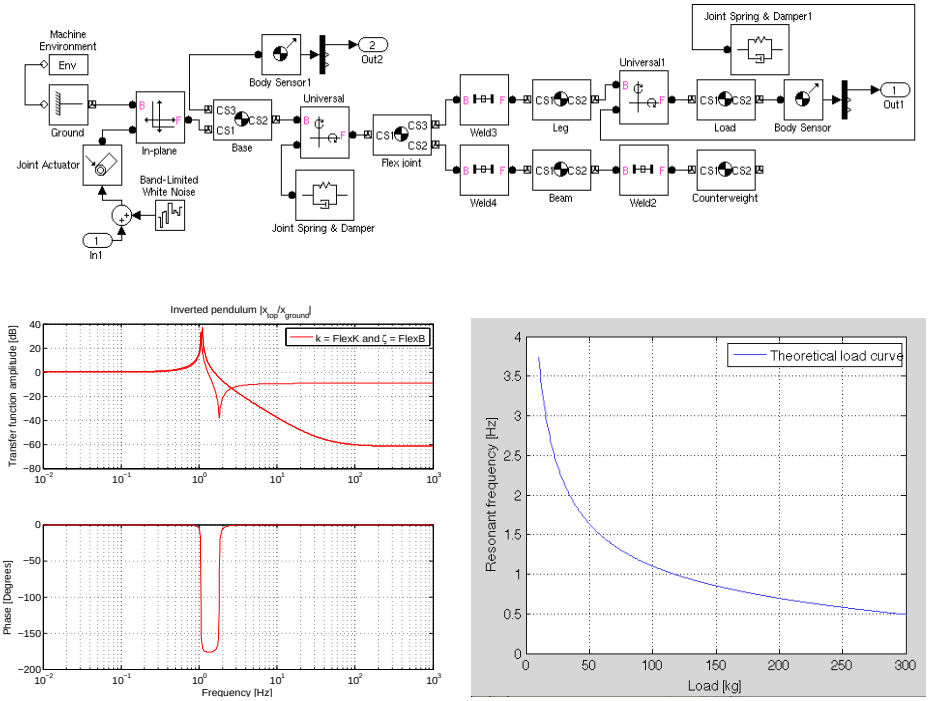

Figure 12: **Top:** SimMechanics model of the inverted pendulum system; **Bottom left:** Bode plots of pendulum dynamics with a counterweight (high amplitude peak) and without a counterweight (lower amplitude peak followed by dip); **Bottom right:** Predicted load curve, from equation 17

4 Towards the Development of a Comprehensive SAS Model

Although comprehensive simulation of the EIB-SAS table is beyond the scope of this report, significant progress has been made towards the goal of simulating and damping the resonances of the complete system. The triple inverted pendulum layer has been fully modeled, along with a robust motion-sensing infrastructure and force feedback control of noise amplification at the resonant frequency of the pendula (see figures 14 and 15).

Motion sensing and force feedback occur in three coordinate systems, each associated with a single pendulum leg. The positions of pendulum legs A, B, and C form equilateral triangles on the table base and top, as shown in figure 14. Motion at each of these points is recorded along an axis parallel to the opposite side of the triangle. In other words, motion at each point is measured along an axis at angle $\theta_A = 0$, $\theta_B = \frac{2\pi}{3}$, or $\theta_C = \frac{4\pi}{3}$ with respect to the positive x-axis of the system environment. Force feedback is calculated for each leg in its own coordinate system. The base and top of the IP layer feature identical sensing systems so that relative motion between the planes can be used in modeling LVDT units and electromagnetic shunt feedback.

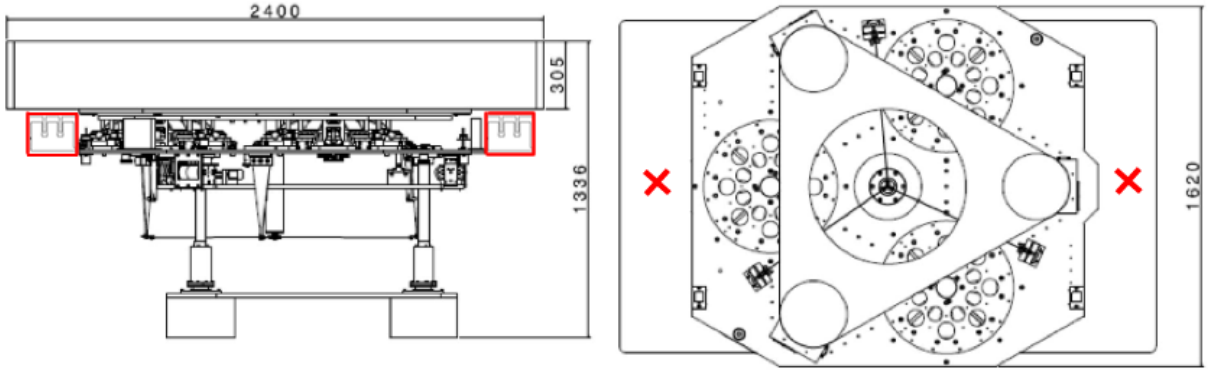

Figure 13: An example of solenoid placement for damping of the second of the EIB-SAS internal modes shown in figure 4. **Left:** Shunt-damped solenoid units are highlighted in red in the side view of the table. **Right:** Solenoid location marked on top view of the table.

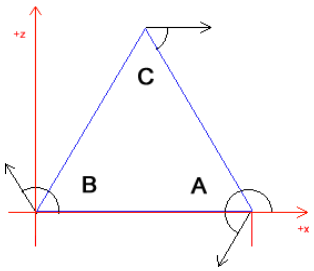

Figure 14: Motion sensing in the EIB-SAS triple inverted pendulum model. $\theta_A = 0$, $\theta_B = \frac{2\pi}{3}$, and $\theta_C = \frac{4\pi}{3}$ with respect to the positive x-axis of the system environment.

A model of the GAS springs layer of the table is currently in development at Nikhef and will be

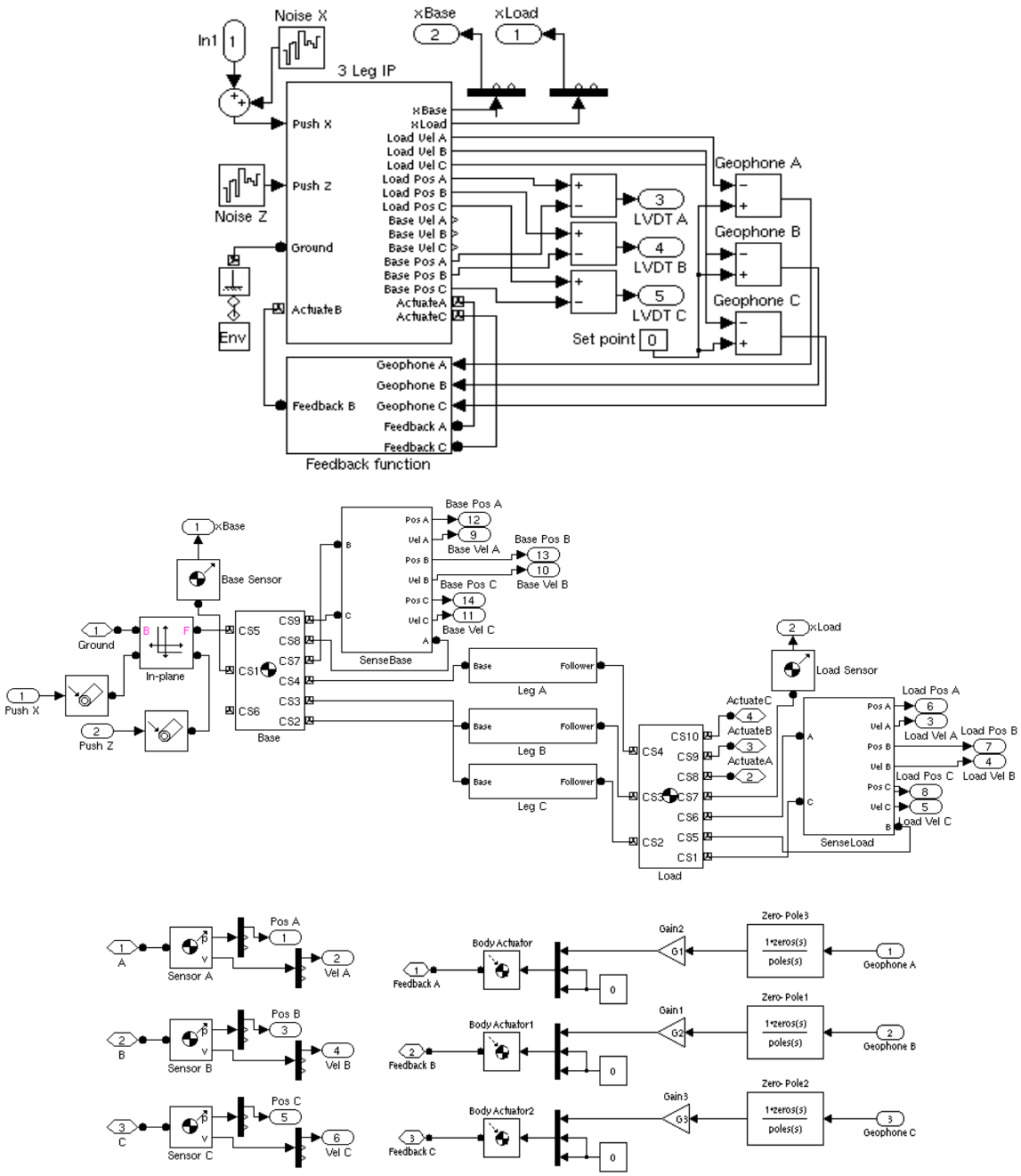

Figure 15: The triple-pendulum layer of the EIB-SAS table. **Top:** Highest level of the system including the triple-IP table as well as models of geophone and LVDT motion signal processing; **Middle:** Subsystem '3 Leg IP' containing pendulum legs, table base, tabletop ('Load'), and motion sensors; **Bottom Left:** Sub-subsystem 'SenseLoad' and 'SenseBase' (the two are identical); **Bottom Right:** Subsystem 'Feedback Function'.

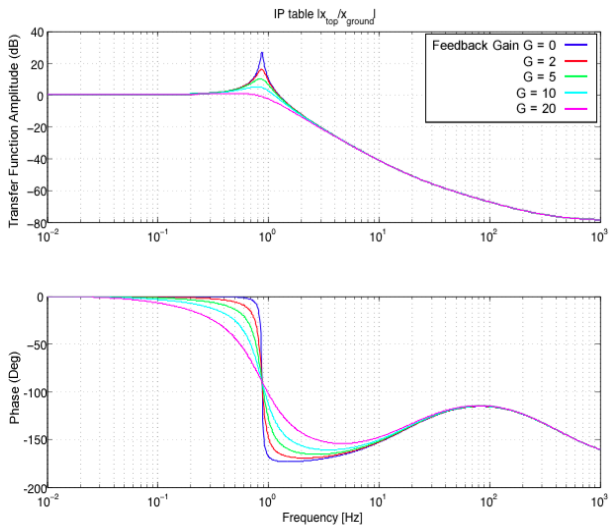

Figure 16: Bode plots for triple IP system with force feedback control to damp amplification at resonance. Varied gain G=0 (blue), 2, 5, 10, 20 (magenta). Counterweights set to 1kg; load mass 1275kg.

combined with the triple pendulum assembly for further testing. Other plans for related work on the EIB-SAS in SimMechanics include continued trials of electromagnetic shunt damping as a control strategy for internal modes. The inverted pendulum resonances, damped by force feedback in the current model, and modes such as those shown in figure 4 are of particular interest as candidates for shunt damping.

5 Conclusion

In this report we have shown that electromagnetic shunt damping is a viable strategy for avoidance of noise amplification by EIB-SAS internal modes. Solenoid shunts are tunable to the various resonant frequencies of the table during the design process, and after installation they provide all the self-regulating advantages of a passive control system. One caveat of this solution is the temperature sensitivity of electrical components; this aspect of the table environment must be controlled in order to maintain damping at the proper frequency.

The EM shunt damping strategy has not yet been directly compared with active force feedback in the SimMechanics triple IP model. However, we can build a shunted solenoid characterized by the same closed-loop transfer function which is currently applied by active feedback in the simulation. Provided that the electromagnetic components are suitably insulated from any nearby conducting materials in the EIB-SAS, replacement of the transfer function by the equivalent physical device will not change the behavior of the damped system, and passive suppression of noise amplification will be achieved.

References

[1] Alex Abramovici and Jake Chapsky. *Feedback Control Systems: A Fast-Track Guide for Scientists and Engineers*. Kluwer Academic Publishers, Dordrecht, The Netherlands, 2000.

[2] John Bechhoefer. Feedback for physicists: A tutorial essay on control. *Reviews of Modern Physics*, 77, 2004.

[3] Valerio Boschi. *Modeling and Simulation of Seismic Attenuation Systems for Gravitational Wave Interferometers*. PhD thesis, University of Pisa, 2010.

[4] Victor Chudnovsky, Arnav Mukherjee, Jeff Wendlandt, and Dallas Kennedy. Modeling flexible bodies in SimMechanics. Technical report, 2006.

[5] Bruno de Marneffe. *Active and Passive Vibration Isolation and Damping via Shunted Transducers*. PhD thesis, Free University of Brussels, 2007.

[6] Arianna di Cintio. Astrophysics issues and low frequency mechanical noise for third generation gravitational wave detectors. Master's thesis, Sapienza University of Rome, 2009.

[7] George P. Gogue and Joseph J. Stupak Jr. Theory and practice of electromagnetic design of DC motors and actuators. Technical report, G2 Consulting, Beaverton, OR, USA, 1993.

[8] Giovanni Losurdo. *Ultra-Low Frequency Inverted Pendulum for the VIRGO Test Mass Suspension*. PhD thesis, The Scuola Normale Superiore of Pisa, 1998.

[9] David S. Rabeling. *Global Sensing and Control for Gravitational Wave Detection*. PhD thesis, The Australian National University, 2009.

[10] D. Robinson. Introduction to feedback control systems. 1994.

[11] Laurent Ruet. *Active Control and Sensor Noise Filtering Duality Application to Advanced LIGO Suspensions*. PhD thesis, Lyon National Institute for Applied Sciences, 2007.

[12] Brett N Shapiro. Modal control with state estimation for Advanced LIGO quadruple suspensions. Master's thesis, The Pennsylvania State University, 2005.

[13] Alberto Stochino. The HAM-SAS seismic isolation system for the Advanced LIGO gravitational wave interferometers. Master's thesis, University of Pisa, 2007.

[14] Jo van den Brand. Nikhef project plan: Benches: Vibration isolation for external benches and suspension of internal benches for Advanced VIRGO. Technical report, Nikhef, National Institute for Subatomic Physics, Amsterdam, The Netherlands, 2010.

[15] Kimmeley van Norel. Internship interim report. 2011.

[16] John Winterflood. *High Performance Vibration Isolation for Gravitational Wave Detection*. PhD thesis, University of Western Australia, 2001.